Neddylation is critical to cortical development by regulating Wnt/β-catenin signaling

Lei Zhang[a], Hongyang Jing[a], Haiwen Li[a], Wenbing Chen[a], Bin Luo[a], Hongsheng Zhang[a], Zhaoqi Dong[a], Lei Li[a], Huabo Su[b], Wen-Cheng Xiong[a,c], and Lin Mei[a,c,1]

[a]Department of Neurosciences, School of Medicine, Case Western Reserve University, Cleveland, OH 44106; [b]Vascular Biology Center, Medical College of Georgia, Augusta University, Augusta, GA 30912; and [c]Louis Stokes Cleveland Veterans Affairs Medical Center, Cleveland, OH 44106

Edited by Richard L. Huganir, The Johns Hopkins University School of Medicine, Baltimore, MD, and approved September 9, 2020 (received for review March 23, 2020)

Wnt signaling plays a critical role in production and differentiation of neurons and undergoes a progressive reduction during cortical development. However, how Wnt signaling is regulated is not well understood. Here we provide evidence for an indispensable role of neddylation, a ubiquitylation-like protein modification, in inhibiting Wnt/β-catenin signaling. We show that β-catenin is neddylated; and inhibiting β-catenin neddylation increases its nuclear accumulation and Wnt/β-catenin signaling. To test this hypothesis in vivo, we mutated Nae1, an obligative subunit of the E1 for neddylation in cortical progenitors. The mutation leads to eventual reduction in radial glia progenitors (RGPs). Consequently, the production of intermediate progenitors (IPs) and neurons is reduced, and neuron migration is impaired, resulting in disorganization of the cerebral cortex. These phenotypes are similar to those of β-catenin gain-of-function mice. Finally, suppressing β-catenin expression is able to rescue deficits of Nae1 mutant mice. Together, these observations identified a mechanism to regulate Wnt/β-catenin signaling in cortical development.

neddylation | Nae1 | Wnt/β-catenin signaling | cerebral cortex | progenitor

The cerebral cortex is characterized by a six-layered structure that is critical to brain function. For example, callosal projection neurons located in layers II/III, V, and VI project their axons to target neurons in the other hemisphere through the corpus callosum to coordinate activities between hemispheres. Subcerebral projection neurons in layer V project to the pons, the superior colliculus, and the spinal cord, to control motor function. Corticothalamic projection neurons in layer VI project axons to thalamus to modulate incoming sensory information (1, 2). This featured lamination is achieved by proliferation and differentiation of radial glial progenitors (RGPs) during cortical development (3). At early embryonic stage, RGPs divide symmetrically in the ventricular zone (VZ) to two daughter RGPs, resulting in progenitor pool expansion. Later, they undergo asymmetric division to one RGP and one neuron (direct neurogenesis) or one intermediate progenitor (IP) (4, 5) or one outer radial glial (oRG) cell (6, 7), which further divide in the subventricular zone (SVZ) to neurons (indirect neurogenesis) (8–10). Sequentially generated neurons migrate radially to form the cortical plate in an inside-out manner, with early-born neurons in deep layers and late-born neurons in upper layers (11, 12). This complex and long process is controlled by several transcription factors, epigenetic regulators, and signaling pathways, including Wnt, Notch, Fgf, and BMP (13).

The Wnt signaling pathway regulates many essential processes in embryonic development, adult tissue homeostasis, and cancer. During embryonic development, Wnt signaling is critical for establishing body axes (14). Wnt signaling can be subdivided into two types: The canonical signaling involves β-catenin-dependent gene transcription which controls stem cell self-renewal, proliferation, and differentiation; the noncanonical pathway is independent on β-catenin and acts via small GTPase and G protein to control cell polarity, movement, and Ca^{2+} signaling (15). Because the Wnt/β-catenin signaling decreases progressively during cortical development (16, 17), β-catenin deletion reduces RGP proliferation, and promotes neuron production (18), but mildly or hardly affects the cortical lamination depending on the different Cre lines used (18–20). In contrast, overexpression of active β-catenin promotes RGP self-renewal, increases apoptosis, and disrupts layer formation (19, 21, 22). However, how the Wnt/β-catenin signaling is regulated during this process is largely unclear.

Neddylation is a posttranslational modification where Nedd8 (neural precursor cell expressed developmentally down-regulated protein 8), a ubiquitin-like molecule, is covalently conjugated to substrate proteins. Similar to ubiquitination, neddylation is catalyzed sequentially by a heterodimer E1 consisting of Nae1 (also known as APP-BP1) and Uba3, an E2 (Ubc12), and various E3s which still need elucidation (23). Activated Nedd8 is covalently conjugated to the lysine residue of target protein through its C-terminal glycine, which can lead to addition of one or more Nedd8 molecules. Neddylation has been implicated in numerous cellular processes, such as transcriptional regulation, receptor tyrosine kinase signaling, apoptosis, DNA damage, and nucleolar stress signaling by changing the localization, activity, or stability of substrate proteins (24). Recently, neddylation is shown to be essential for adipogenesis (25) and heart development (26). In the developing nervous system, neddylation increases during maturation and promotes dendritic spine maturation, synaptic transmission, and neuromuscular junction formation (27–29).

Significance

The neocortex is characterized by a six-layered structure that is critical to brain function. Cortical development requires proper generation and differentiation of neurons that migrate out from the ventricular zone to populate the cortex. This is regulated by Wnt/β-catenin signaling, which reduces gradually during cortical development. However, how the decreasing of Wnt/β-catenin signaling is regulated is largely unclear. We demonstrate that neddylation, a ubiquitylation-like protein posttranslational modification, targets β-catenin itself to inhibit Wnt/β-catenin signaling in the process. We also show that ablating Nae1, an obligative subunit of the E1 for neddylation, from cortical progenitor cells leads to similar phenotypes in β-catenin gain-of-function mice. This study reveals a previously unappreciated role of neddylation in regulating cortical lamination by targeting β-catenin signaling.

Author contributions: L.Z., W.-C.X., and L.M. designed research; L.Z., H.J., H.L., W.C., B.L., H.Z., Z.D., and L.L. performed research; H.S. contributed new reagents/analytic tools; L.Z., H.J., H.L., W.C., and B.L. analyzed data; and L.Z. and L.M. wrote the paper.

The authors declare no competing interest.

This article is a PNAS Direct Submission.

[1]To whom correspondence may be addressed. Email: lin.mei@case.edu.

This article contains supporting information online at https://www.pnas.org/lookup/suppl/doi:10.1073/pnas.2005395117/-/DCSupplemental.

First published October 5, 2020.

Thus, the changes of Wnt/β-catenin signaling and neddylation of substrates during development suggest that they might be negatively correlated. In this study, we found that neddylation suppresses Wnt/β-catenin signaling by targeting β-catenin in vitro. Remarkably, inhibition of neddylation by ablating Nae1 from cortical progenitors disorganized and thinned the cerebral cortex, suggesting a critical role of neddylation in cortical lamination. We characterized the effect of Nae1 mutation on the expression of markers of RGPs and IPs and the proliferation status of these cells. Results suggest that Nae1 mutation impairs the generation and migration of neurons and thus disrupts the cortical lamination, which is similar to those found in β-catenin gain-of-function mutant mice. In accord, β-catenin signaling was increased in cortex of Nae1 conditional knockout (CKO) mice and knockdown of β-catenin partially rescues the increase of RGP proliferation. Taken together, these results reveal a previously unappreciated role of neddylation in regulating cortical development by directly controlling β-catenin signaling.

Results

Neddylation Directly Inhibits β-Catenin Signaling. Wnt/β-catenin signaling is critical for cortical development (13) and undergoes progressive reduction during the process (16), while the neddylation of substrates in brain or cultured neurons increases during maturation (27). This suggests Wnt/β-catenin signaling and neddylation are negatively correlated. To test whether Wnt/β-catenin signaling is regulated by neddylation, we incubated HEK293T cells with MLN-4924, an inhibitor of Nae1 (30), and checked possible changes of β-catenin. Cells were fractioned into cytoplasmic fractions (positive for α-tubulin) and nuclear fractions (positive for PARP, poly [ADP ribose] polymerase) (*SI Appendix*, Fig. S1*A*). MLN-4924 reduced the level of neddylated proteins at ∼90 kDa, a molecular weight of Cullins, well-characterized substrates of neddylation (*SI Appendix*, Fig. S1*A*) (31). Remarkably, β-catenin levels were increased in both cytoplasmic and nuclear fractions of MLN-4924-treated HEK293T cells (*SI Appendix*, Fig. S1*A*). To test the functional outcome of increased β-catenin, we transfected TOP-Flash in HEK293T cells and treated them with MLN-4924. As shown in *SI Appendix*, Fig. S1*B*, the luciferase activity was increased in cells treated with MLN-4924, relative to those with vehicle. These data indicate that neddylation inhibition promotes β-catenin signaling. To determine how neddylation alters the levels of β-catenin, we treated HEK293T cells with cycloheximide (CHX), a protein translation inhibitor, and monitored β-catenin levels over time. As shown in *SI Appendix*, Fig. S1*C*, β-catenin level reduction was slowed in cells treated with MLN-4924, indicating that neddylation may regulate the stability of β-catenin.

Next, to determine whether β-catenin might be the direct target for neddylation, we transfected HEK293T cells with Flag-tagged β-catenin and HA-tagged Nedd8. Lysates were subjected to precipitation with anti-Flag antibody to isolate β-catenin, which was then probed with anti-Nedd8 antibody. As shown in Fig. 1*A*, immunoreactivity was increased in cells cotransfected with both Flag-β-catenin and HA-Nedd8, by not individually. Importantly, the signal was attenuated when cells were incubated with MLN-4924 (Fig. 1*A*). Because in neddylation, Nedd8 is covalently conjugated to substrate proteins through two glycine residues at the C-terminal (32), we determined whether β-catenin neddylation could be diminished by Nedd8ΔGG. As shown in Fig. 1*B*, indeed, β-catenin was no longer neddylated when cells were cotransfected with Nedd8ΔGG. Furthermore, neddylation of β-catenin was reduced in cells cotransfected with Nedp1, a deneddylase (33) (Fig. 1*C*). Finally, neddylation of endogenous β-catenin was detectable in HEK293T cells when cell lysates were precipitated with anti-β-catenin antibody followed by probing with anti-Nedd8 antibody (Fig. 1*D*). These data indicate β-catenin can be neddylated in HEK293T cells.

Noticeably, a recent proteomic analysis identified β-catenin as a neddylated protein and identified several potential neddylated lysine residues (34). We next examined which of these lysines may be neddylated. To this end, we generated point lysine-to-arginine mutations and tested whether they change the neddylation level of β-catenin. Western blots following immunoprecipitation showed a decrease of β-catenin neddylation by K19R, K170R, K233R, K354R, and K625R (Fig. 1*E*), identifying five potential neddylation residues in β-catenin. Finally, we tested whether the cellular localization of β-catenin could be regulated by neddylation and transfected HEK293T cells with β-catenin wild type and mutants. Compared with wild type, mutations such as K170R, K233R, and K354R increased the levels of β-catenin in nuclear fractions (Fig. 1*F*), suggesting neddylation may prevent β-catenin from nuclear localization. To test this hypothesis further, we examined the effects of the lysine-arginine mutations on subcellular distribution of β-catenin. In agreement with Western blot analysis, β-catenin levels in the nuclei were increased by K170R and K233R (Fig. 1 *I*, *J*, and *M*). K354R showed a trend of nuclear enrichment but failed to reach statistical significance (Fig. 1 *K* and *M*). We also noticed that although K19R and K625R reduced the neddylation level of β-catenin, their nuclear enrichment was not significantly higher than wild-type controls. Perhaps this could suggest that neddylation may be regulated by additional mechanisms that are yet to be identified. Together, these data indicate that β-catenin nuclear localization could be regulated by neddylation.

Disorganized Neocortex and Cortical Lamination in Nae1 Mutant Mice. Having shown that neddylation directly and negatively regulates β-catenin signaling, we determined whether the effect of inhibiting neddylation in cortical development is similar to that found in β-catenin gain-of-function mice. To this end, we chose to delete Nae1, the obligative subunit of neddylation E1 and thus examined its expression in the cerebral cortex using in situ hybridization (ISH) at embryonic day (E) 18.5, when cortical neurogenesis almost terminates (*SI Appendix*, Fig. S2*A*). Nae1 mRNA was detected by antisense probes in postmitotic neurons of cortical plate (CP), the presumptive layer II to VI, as well as SVZ/VZ, where the cortical progenitors reside (*SI Appendix*, Fig. S2 *B* and *C*). Nae1 mRNA was relatively low in the intermediate zone (IZ) containing migrating neurons from SVZ/VZ to CP (*SI Appendix*, Fig. S2 *B* and *C*). As control, no signal was detected by sense probes (*SI Appendix*, Fig. S2*C*). These data indicate Nae1 is expressed in cortical progenitors and neurons, in agreement with a previous report (35). We crossed floxed Nae1 with Emx1-Cre mice (*SI Appendix*, Fig. S2*D*), a line where Cre recombinase is expressed under the control of the endogenous Emx1 promoter that is active in cortical progenitors since E10.5 (36). The offspring of Emx1-Cre::Nae1$^{f/f}$ mice were referred to as Nae1 CKO mice, and their littermates Nae1$^{f/+}$ or Nae1$^{f/f}$ mice were used as control. Nae1 protein was dramatically reduced in cortical samples of Nae1 CKO mice at E15.5, a peak of cortical neurogenesis (*SI Appendix*, Fig. S2*E*), indicating successful establishment of this CKO mouse line. Nae1 CKO mice died prematurely before postnatal day (P) 28 (*SI Appendix*, Fig. S2*F*). Nae1 CKO mice showed a decrease of Nedd8-conjugated proteins (*SI Appendix*, Fig. S2 *G* and *H*), and in particular, a down-regulation of neddylated Cul1, a protein known to be neddylated (*SI Appendix*, Fig. S2 *G* and *H*).

We next examined the impact of Nae1 deletion on cortical morphology by Nissl staining. At P0 (Fig. 2 *A* and *B*), a stage when cortical neurogenesis finishes, Nae1 CKO mice showed thinner cortex and enlarged lateral ventricle (Fig. 2 *C*, *E*, and *G*). In particular, the hippocampus was tiny with no identifiable cornu ammonis (CA) and dentate gyrus (DG) regions (Fig. 2 *C* and *E*). Besides thinning, the cortex in Nae1 CKO mice was disorganized without clear lamination (Fig. 2 *D* and *F*). These results demonstrate a critical role of neddylation in cortical development. To further test this notion, we studied the cortex at a

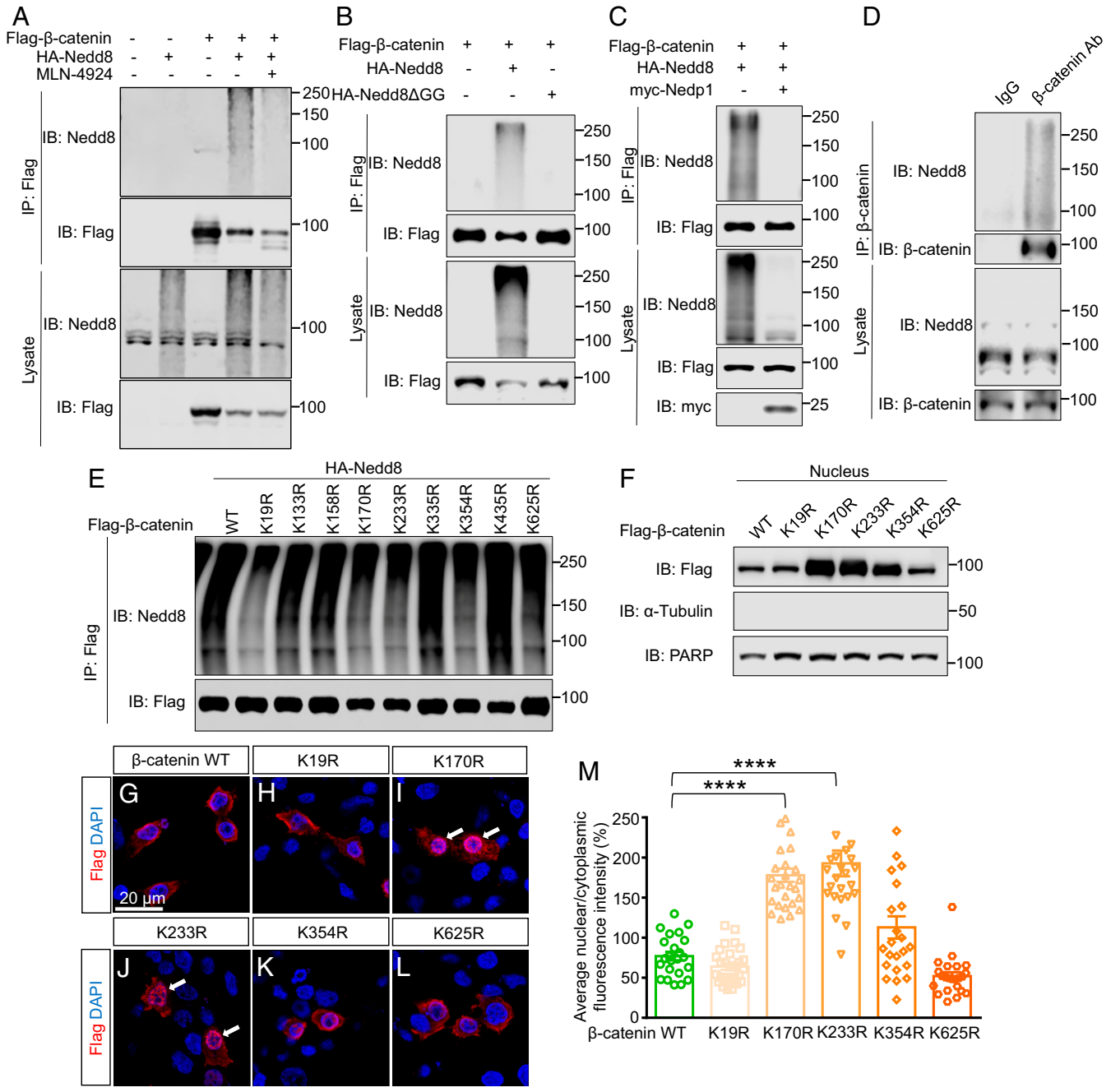

Fig. 1. Neddylation of β-catenin in HEK293T cells. (*A*) Neddylation of β-catenin is detected by immnoprecipitation and Western blots in HEK293T cells. Cells are transfected with Flag-β-catenin, HA-Nedd8, or both without or with MLN-4924. This neddylation is reduced in the presence of MLN-4924. (*B*) Neddylation of β-catenin is abolished when cells are transfected with Flag-β-catenin and a conjugation-inable mutant Nedd8 (HA-Nedd8ΔGG). Neddylation of β-catenin is revealed as in *A*. (*C*) Neddylation of β-catenin is dramatically reduced when cells are transfected with Flag-β-catenin, HA-Nedd8, and a deneddylase myc-Nedp1. Neddylation of β-catenin is revealed as in *A*. (*D*) Neddylation of β-catenin is detected in endogenous β-catenin of HEK293T cells using immunoprecipitation and Western blots. (*E*) Neddylation of β-catenin is reduced using immunoprecipitation and Western blots when HEK293T cells are transfected with some site mutants. Cells are transfected with HA-Nedd8 and WT Flag-β-catenin or one of the site-mutant β-catenin plasmids. Neddylation level of β-catenin-K19R, K170R, K233R, K354R, and K625R is reduced. (*F*) β-Catenin site-mutant proteins (K170R, K233R, and K354R) are increased in cell nuclei as shown by Western blots. Cells are transfected with Flag-β-catenin-WT, K19R, K170R, K233R, K354R, or K625R and higher levels of β-catenin-K170R, K233R, and K354R are found in nuclear fraction. α-Tubulin and PARP serve as markers for cytoplasmic and nuclear fraction, respectively. (*G–L*) β-Catenin site-mutant proteins (K170R and K233R) are accumulated in cell nuclei as shown by immunostaining. Cells are transfected with Flag-β-catenin-WT, K19R, K170R, K233R, K354R, or K625R. Fluorescence of Flag is found to be accumulated in β-catenin-K170R and K233R. Arrows indicate elevated nuclear fluorescence of Flag (Scale bar, 20 μm.) (*M*) Quantitation of Flag fluorescence intensity in cell nuclei relative to cytoplasm. Data are shown as mean ± SEM ****$P < 0.0001$, one-way ANOVA with post hoc Dunnett's test. $n = 23$ to 29 for different groups.

later age, P7 (*SI Appendix*, Fig. S3 *A* and *B*). Similarly, cortical thinning, enlarged ventricle, tiny hippocampus, and disorganized cortex were observed in Nae1 CKO mice (*SI Appendix*, Fig. S3 *C–G*). Besides, the corpus callosum was lost in mutant mice (*SI Appendix*, Fig. S3 *C* and *E*). These data indicate that cortical development was affected by Nae1 mutation and suggest that neddylation is required for normal cortical lamination.

To understand cellular mechanisms by which neddylation regulates cortical lamination, cortical sections were immunostained for neuronal markers of different layers at E14.5, around peak of cortical neurogenesis (Fig. 2*H*). In control mice, cells positive for Tuj1, a pan-neuronal marker that labels early-born neurons and migrating immature neurons (37), were distributed in SVZ and CP (Fig. 2 *I*, *a* and b). Many neurons in the CP were positive for Ctip2 (Fig. 2 *I*, *a* and *b*), a marker of layer V/VI (deep layers) neurons (38). At E16.5 (Fig. 2*K*), Tuj1$^+$ cells appeared on top of the CP and in the expanded IZ and SVZ (Fig. 2 *L*, *a* and *b*). On the other hand, Ctip2$^+$ neurons remain in the deeper CP (Fig. 2 *L*, *a* and *b*). At E17.5 (Fig. 2*P*), cells positive for Cux1, a marker of neurons in layer II to IV (upper layers) (39), were located in the upper CP (i.e., between the pia and deeper CP) (Fig. 2 *Q*, *a* and *b*). The IZ was populated with migrating neurons positive for Tuj1 or Cux1 (Fig. 2 *L*, *b* and *Q*, *b*). These results showed a classic inside-out pattern of cortical neuron migration (40). However, in Nae1 CKO mouse brains, the number of Ctip2$^+$ cells was reduced at E14.5 and E16.5 (Fig. 2 *J*, *a* and *b*, *M*, *a* and *b*, and *N*), suggesting a problem with neurogenesis. Remaining Ctip2$^+$ cells appeared to form clusters in the CP and deeper CP (Fig. 2 *J*, *b* and *M*, *b*, respectively). Cells below the CP or deeper CP were not positive for Tuj1 (Fig. 2 *J*, *b*, *M*, *b*, and *O*), indicating severe reduction of migrating neurons, in agreement with the notion that neurogenesis was reduced. At E17.5, the number of both Ctip2$^+$ and Cux1$^+$ neurons were reduced overall (Fig. 2 *R–T*); noticeably, few if any Cux1$^+$ neurons were detectable in the layer above the deeper CP (Fig. 2 *R*, *a* and *R*, *b*), effectively eliminating the upper CP. Because cells below the deeper CP could not be labeled by Tuj1, a marker of migrating neurons, a parsimonious interpretation of these results is that Nae1 mutation reduced neurogenesis.

Reduced Cortical Neurons and Astrocytes by Nae1 Mutation. To investigate the impact of Nae1 mutation on the cortical neurons and astrocytes in postnatal mouse brains, we checked the expression of NeuN (neuronal marker), AldoC and GFAP (both are astrocytic markers) at P4. In control mice (Fig. 3 *A* and *B*), NeuN$^+$ cells were densely distributed in all layers of the cortex (Fig. 3 *C* and *D*), while in Nae1 CKO mice (Fig. 3 *L* and *M*), the layer I and subplate (SP) were lost (Fig. 3 *E* and *F*). The mRNA of Reelin revealed by ISH and Calretinin by immunostaining, both markers of layer I interneurons, were diminished in the superficial layer of Nae1 CKO mice (*SI Appendix*, Fig. S4 *G–L*). NeuN$^+$ cells were dispersedly located in the cortex (Fig. 3 *E* and *F*). Further, many NeuN$^+$ neurons formed clusters in the mutant cortex (arrows in Fig. 3*F*). Our results also showed NeuN$^+$ neuronal number or cell density was decreased (Fig. 3 *C–G*), suggesting the neurogenesis in Nae1 CKO mice was impaired.

For glial cells, we performed AldoC (astrocyte marker) and GFAP (marker for both activated astrocytes and RGPs) double immunostaining. In control mice (Fig. 3 *A* and *B*), AldoC$^+$ astrocytes were evenly distributed in all layers of the cortex (Fig. 3 *H* and *I*). Immunostaining of GFAP labeled not only activated astrocytes around layer I and white matter, but also RGPs with apparent radial fibers extending to the pial surface (Fig. 3 *H* and *I*), while in Nae1 CKO mice (Fig. 3 *L* and *M*), AldoC$^+$ astrocytes or GFAP$^+$ activated astrocytes (arrows indicate remaining astrocytes in Fig. 3*K*) were rarely observed in the cortex (Fig. 3 *J*, *K*, and *N*). RGPs were completely lost in the VZ by absence of any radial fibers in the cortex (Fig. 3*K*). To determine whether these scaffolds were impaired before P0, we examined the radial fibers by immunostaining of Nestin (marker for RGPs) at E14.5 and E17.5 (*SI Appendix*, Fig. S4 *A* and *D*). At E14.5, the Nestin$^+$ fibers in the cortex were comparable between control and Nae1 CKO mice (*SI Appendix*, Fig. S4 *B* and *C*). While at E17.5, many fibers extending radially to the pial surface were observed in control brains (*SI Appendix*, Fig. S4*E*), but these fibers underwent a dramatic reduction, leaving only a few in the cortex of Nae1 CKO mice (*SI Appendix*, Fig. S4*F*). These data indicate radial fibers of RGPs in Nae1 mutants are impaired at E17.5. Taken together, these results indicate a decrease of cortical neurons and astrocytes postnatally, suggesting the defects in cortical neurogenesis at embryonic stages.

Reduced RGPs and IPs in Nae1 CKO Mice. The reduced neurons in Nae1 CKO cortex may be due to 1) abnormal proliferation/differentiation of cortical progenitors, 2) increase of cell apoptosis, and/or 3) impaired migration. Thus, we checked the cortical progenitors and their proliferation and differentiation. RGPs are a major type of cortical progenitors, which generate neurons directly or generate IPs first and then neurons (Fig. 4*M*) (41). We stained cortical sections with antibodies against Sox2 (a marker for RGP) and Tbr2 (a marker for IP). Sox2$^+$ cells were unchanged at E14.5, increased at E16.5, but eventually reduced at E18.5, compared with controls (Fig. 4 *A–G*). On the other hand, Tbr2$^+$ cells were reduced at both E14.6 and E16.5, suggesting impaired generation of IPs and identifying a mechanism of neuron reduction. To investigate mechanisms of the transient increase in Sox2$^+$ cells at E16.5, we examined the expression of phosphohistone H3 (PH3), a mitotic marker at the same stages (Fig. 4*N*). Because RGPs undergo cell division (i.e., mitosis) at the apical surface of the VZ, and IPs are in the SVZ and VZ (except the apical surface of the VZ) (Fig. 4*M*) (42), PH3$^+$ cell counts were quantitated based on cell location (VZ surface and non-VZ surface). Comparable numbers of PH3$^+$ cells at the VZ surface were observed between control and Nae1 CKO mice at E14.5 (Fig. 4 *O* and *Q*), in agreement with the observation of no change in Sox2$^+$ cells at this age. However, fewer positive cells for PH3 were observed at non-VZ surface in Nae1 CKO mice (Fig. 4 *O* and *R*), compared with control mice. These results suggest that Nae1 mutation inhibits self-renewal of IPs at E14.5. Intriguingly, the number of PH3$^+$ cells at the VZ surface was increased at E16.5, compared with control mice (Fig. 4 *P* and *Q*), indicative of elevated proliferation of RGPs (Fig. 4 *D* and *G*). To further test this hypothesis, we labeled cells with a single pulse of bromodeoxyuridine (BrdU) at E15.5. Mice were killed 24 h later (Fig. 4*S*) and brain slices were immunostained for Ki67 (a cell cycle marker) and BrdU (Fig. 4*T*). The ratio of BrdU$^+$Ki67$^+$ cells to total BrdU$^+$ cells was increased in Nae1 CKO brains, compared to that of control mice (Fig. 4*U*), suggesting a decrease in cell cycle exit. Finally, we examined the cleavage plane orientation of mitotic RGPs at E14.5 when phenotypes were observed in Nae1 mutant mice and also at E11.5, a time when phenotypes were not observed. However, there was no change of cleavage plane orientation at both times (*SI Appendix*, Fig. S5), suggesting little RGP switch from asymmetric division to symmetric division in Nae1 CKO cortex. These data indicate that increased RGP proliferation at E16.5 in Nae1 CKO mice is likely due to reduced cell cycle exit.

Notice that RGPs were reduced at E18.5 (Fig. 4 *F* and *G*). To investigate underlying mechanisms, we immunostained for cleaved Caspase-3 (a marker for apoptosis). At E14.5, apoptotic cells in Nae1 CKO mouse brains were similar to that in controls (Fig. 4 *V*, *W*, and *Z*). However, at E16.5, many cells became positive for cleaved Caspase-3, and the apoptotic cells were localized in the VZ and SVZ, in contrast to controls with few positive cells (Fig. 4 *X* and *Z*). Enhanced Wnt/β-catenin activity has been shown to cause DNA damage in different cell types, including intestinal stem and

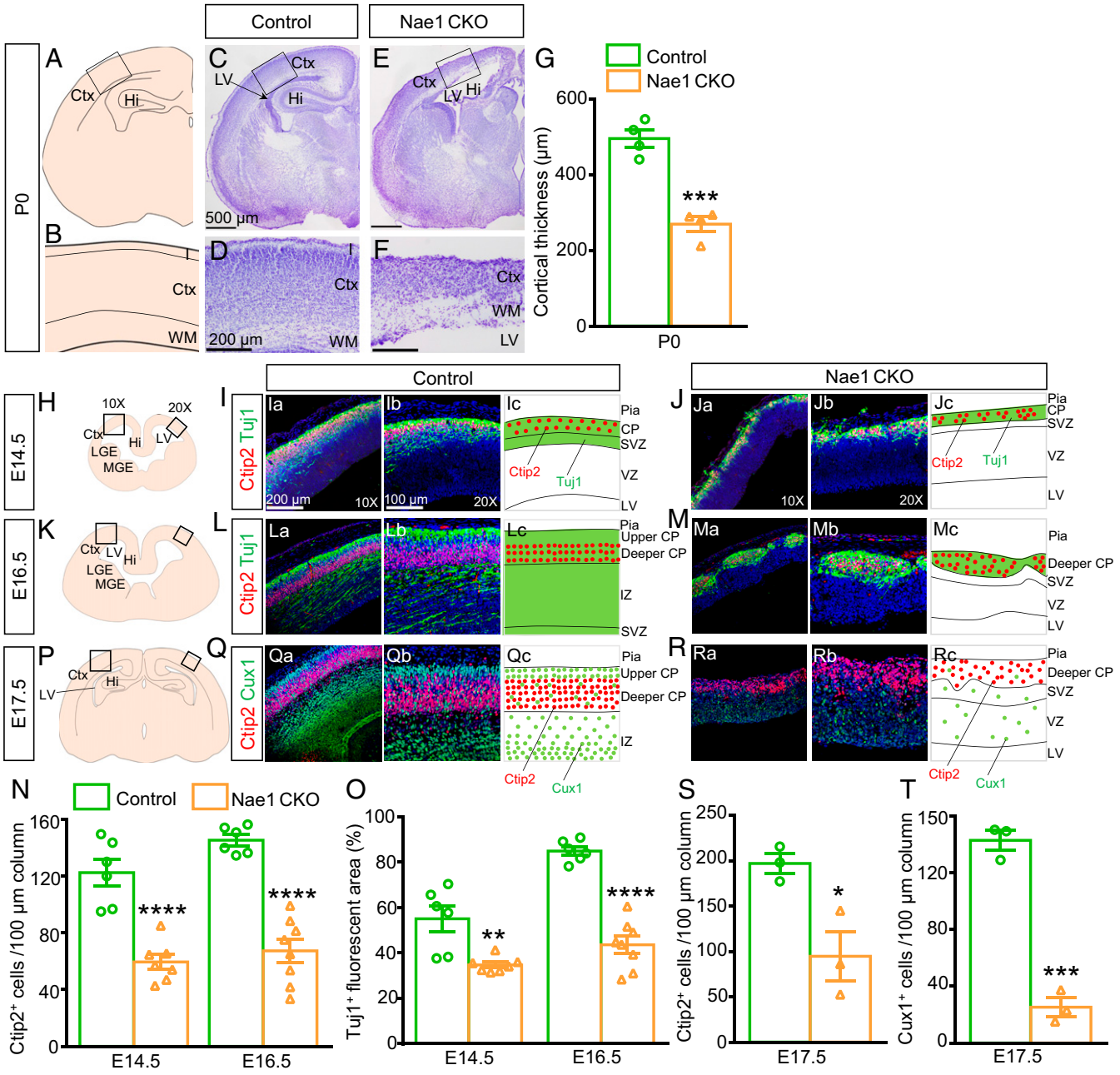

Fig. 2. Cortical disorganization and lamination deficits in Nae1 CKO mice. (*A* and *B*) Diagrams of coronal brain section at P0. The boxed area in *A* is enlarged in *B*. Ctx, cortex; Hi, hippocampus; I, layer I; WM, white matter. (*C–F*) Nae1 CKO mice show thinner cerebral cortex, loss of hippocampus, and disrupted cortical organization at P0 by Nissl staining. *D* and *F* are from boxed areas in *C* and *E*, respectively. LV, lateral ventricle. (*G*) Quantitation of cortical thickness at P0. Data are shown as mean ± SEM ***$P < 0.001$, Student's *t* test, $n = 4$. (*H–J*) Fewer deep-layer neurons and immature migrating neurons in Nae1 CKO mice at E14.5. (*H*) Diagram of coronal brain sections of mice at E14.5. The large boxed area (10×) corresponds to *Ia* and *Ja*, the small boxed area (20×) to *Ib* and *Jb*. *Ic* and *Jc* show schematic diagrams of phenotypes in control and Nae1 CKO mice, respectively. Immunostaining of Ctip2 (deep-layer neuronal marker) and Tuj1 (pan-neuronal marker) shows that Ctip2$^+$ cells and the Tuj1$^+$ area were decreased at E14.5. Red dots represent Ctip2$^+$ cells and green regions represent Tuj1$^+$ area. LGE, lateral ganglionic eminence; MGE, medial ganglionic eminence; Pia, pial surface; CP, cortical plate; SVZ, subventricular zone; VZ, ventricular zone; IZ, intermediate zone. (*K–M*) Fewer deep-layer neurons and immature migrating neurons in Nae1 CKO mice at E16.5. (*K*) Diagram of coronal brain sections of mice at E16.5. The large boxed area (10×) corresponds to *La* and *Ma* and the small boxed area (20×) to *Lb* and *Mb*. *Lc* and *Mc* show schematic diagrams of phenotypes in control and Nae1 CKO mice, respectively. (*N* and *O*) Quantitation of Ctip2$^+$ cells per 100-μm cortical column and Tuj1$^+$ area (%). Data are shown as mean ± SEM **$P < 0.01$, ****$P < 0.0001$, Student's *t* test. For control mice, $n = 6$ at E14.5 and E16.5. For Nae1 CKO mice, $n = 7$ at E14.5 and $n = 8$ at E16.5. (*P–R*) Fewer deep-layer neurons and loss of upper-layer neurons in Nae1 CKO mice at E17.5. (*P*) Diagram of coronal brain sections of mice at E17.5. The large boxed area (10×) corresponds to Qa and Ra and the small boxed area (20×) to *Qb* and *Rb*. *Qc* and *Rc* show schematic diagrams of phenotypes in control and Nae1 CKO mice, respectively. Immunostaining of Ctip2 and Cux1 (upper-layer neuronal marker) shows decrease of Ctip2$^+$ cells and loss of Cux1$^+$ cells superficial to Ctip2$^+$ cells. Red dots represent Ctip2$^+$ and green dots represent Cux1$^+$ cells. (*S* and *T*) Quantitation of Ctip2$^+$ and Cux1$^+$ cells per 100-μm cortical column. Data are shown as mean ± SEM *$P < 0.05$, ***$P < 0.001$, Student's *t* test, $n = 3$ (Scale bars, 500 μm in *C* and *E*, 200 μm in *D* and *F*, 200 μm in *I*, *J*, *L*, *M*, *Q*, and *Ra* and 100 μm in *I*, *J*, *L*, *M*, *Q*, and *Rb*.)

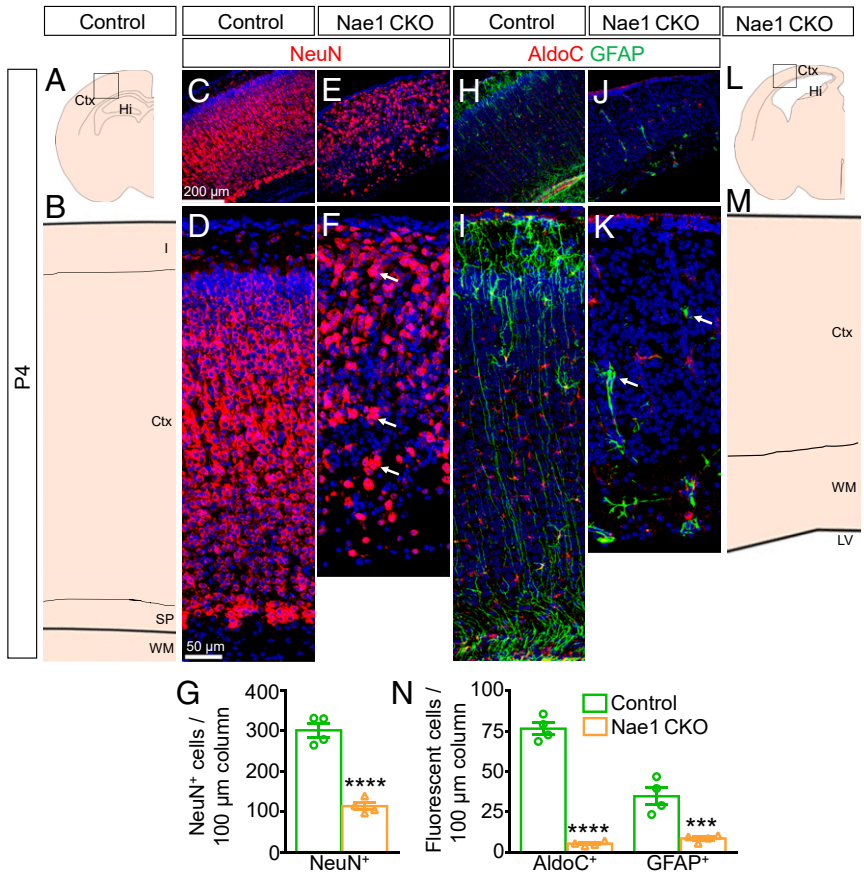

Fig. 3. Decreased neurons and astrocytes in Nae1 CKO mice. (*A* and *B*) Diagrams of control coronal brain sections at P4. The boxed area in *A* corresponds to *C* and *H*. The *B* corresponds to *D* and *I*. Ctx, cortex; Hi, hippocampus; I, layer I; SP, subplate; WM, white matter. (*C–F*) The number of NeuN$^+$ neurons shown by immunostaining is decreased in Nae1 CKO mice at P4. The arrows in *F* indicate clustering of some NeuN$^+$ cells. Note the lack of layer I and subplate in Nae1 CKO mouse cortex. (*G*) Quantitation of NeuN$^+$ cells per 100-μm cortical column at P4. Data are shown as mean ± SEM ****$P < 0.0001$, Student's *t* test, $n = 4$. (*H–K*) The number of AldoC$^+$ astrocytes and GFAP$^+$ RGPs/activated astrocytes shown by immunostaining is dramatically decreased in Nae1 CKO mice at P4. The arrows in *K* indicate remaining GFAP$^+$ cells with abnormal morphology. (*L* and *M*) Diagrams of coronal brain sections of Nae1 CKO mice at P4. The boxed area in *A* corresponds to *E* and *J*. The *B* corresponds to *F* and *K*. LV, lateral ventricle. (*N*) Quantitation of AldoC$^+$ and GFAP$^+$ cells per 100-μm cortical column at P4. Data are shown as mean ± SEM ***$P < 0.001$, ****$P < 0.0001$, Student's *t* test, $n = 4$ (Scale bars, 200 μm in *C*, *E*, *H*, and *J* and 50 μm in *D*, *F*, *I*, and *K*.)

progenitor cells and mesenchymal stem cells (43, 44). In accordance with this, we show that γH2AX, a marker of DNA damage, was increased in Nae1 CKO mice (*SI Appendix*, Fig. S6 *A–D*). DNA damage is known to induce apoptosis (45). Indeed, enhanced Wnt/β-catenin signaling has been shown to increase apoptosis in cerebral cortex, hematopoietic stem/progenitor cells, and melanoma cells (19, 46, 47). Nae1 inhibition has been shown to induce DNA damage (48). To determine whether β-catenin neddylation regulates apoptosis, we expressed mutated K170 and K233, two major sites of neddylation (Fig. 1 *E–M*), in HEK293T cells. As shown in *SI Appendix*, Fig. S6*F*, their expression increased p53, a protein which is critical for DNA damage response and apoptosis (49). These results support the hypothesis that loss of neddylation in β-catenin might increase DNA damage and apoptosis through the p53-dependent pathway.

Reduced Differentiation of Nae1-Deficient Progenitor Cells. To investigate the impact of Nae1 mutation on progenitor cell differentiation, we labeled cortical progenitors with EGFP by in utero electroporation (IUE) at E14.5 (50). BrdU was then administered once at E15.5 to label dividing progenitors, and brains were dissected out 1 d later (Fig. 5*A*). Brain slices were immunostained for different proliferation and progenitor markers as mentioned above (Fig. 5*B*). In control mice, most EGFP-labeled cells exited the cell cycle and migrated to the IZ, and some even reached the cortical plate with typical bipolar morphology of migrating neurons (Fig. 5 *C* and *F*). Most of the control cells were located above the BrdU- or Sox2-labeled zone, with the ratio of double-labeled cells to GFP$^+$ cells around 20% (Fig. 5 *C*, *E*, *F*, and *H*). In Nae1 CKO mice, most GFP$^+$ cells resided in BrdU- or Sox2-labeled zone, and about 50% or 60% of total GFP-labeled cells were BrdU$^+$ or Sox2$^+$, respectively (Fig. 5 *D*, *E*, *G*, and *H*). These results indicate most of the mutant cells are still RGPs even 2 d after being labeled. Similarly, most of GFP-labeled cells migrated out of Tbr2$^+$ SVZ/VZ and only 10% of GFP$^+$ cells were Tbr2$^+$ IP (Fig. 5 *I* and *K*), while GFP-labeled mutant cells were almost beneath the Tbr2$^+$ area and showed a decreased ratio of double-positive cells to total GFP$^+$ cells (Fig. 5 *J* and *K*). These data suggest the differentiation from RGP to IP reduces in Nae1 CKO mouse brains. As mentioned before, the PH3$^+$ mitotic cell portion showed a drastic increase between control and Nae1 CKO mice (Fig. 5 *L–N*), which is consistent with the increase of BrdU$^+$ or Sox2$^+$ cells at this stage. The diagrams illustrating the distribution of control and Nae1 mutant cells are shown in Fig. 5 *O* and *P*. Taken together, our data indicate that Nae1 mutant cells maintain themselves in the progenitor state instead of differentiation.

Rescuing Cortical Deficits in Nae1 CKO Mice by Suppressing β-Catenin. β-Catenin gain of function increases apoptosis of cortical progenitor cells and decreases the IPs and the thickness of cortex

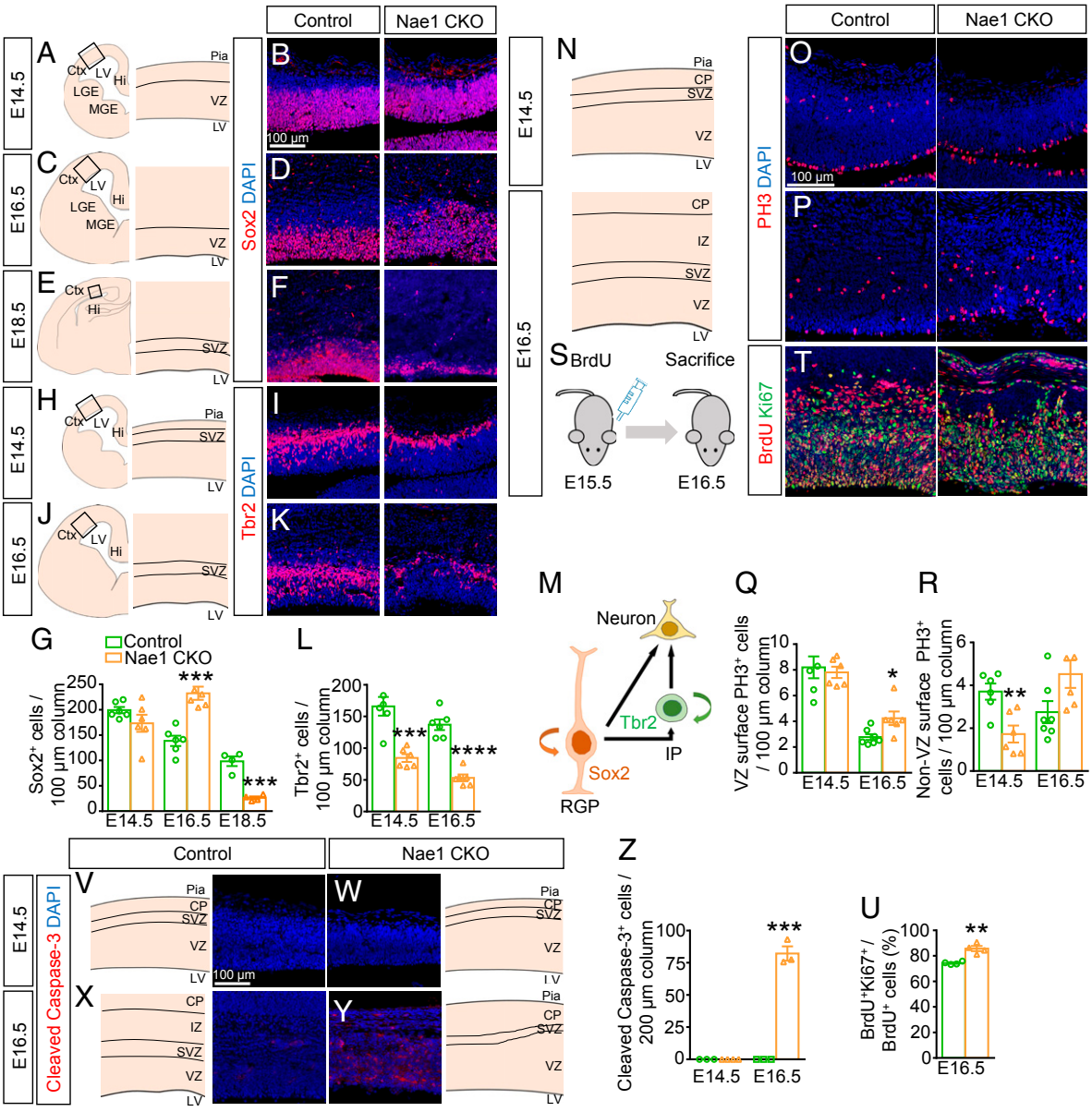

Fig. 4. Reduced RGPs and IPs in Nae1 CKO mice. (*A*) Diagram of coronal brain sections at E14.5. The *Right* in *A* is from boxed area on the *Left*. Ctx, cortex; LV, lateral ventricle; Hi, hippocampus; LGE, lateral ganglionic eminence; MGE, medial ganglionic eminence; Pia, pial surface; VZ, ventricular zone. (*B*) Immunostaining of Sox2 (marker for RGP) shows normal RGPs between control and Nae1 CKO mice at E14.5. The position of *B* corresponds to the boxed area in *A*. (*C*) Diagram of coronal brain sections at E16.5. The *Right* in *C* is from boxed area on the *Left*. (*D*) RGPs are increased in Nae1 CKO mice. Immunostaining of Sox2 shows elevated number of positive cells at E16.5. The position of *D* corresponds to the boxed area in *C*. (*E*) Diagram of coronal brain sections at E18.5. The *Right* in *E* is from boxed area on the *Left*. (*F*) RGPs are decreased in Nae1 CKO mice. Immunostaining of Sox2 shows reduced number of positive cells at E18.5. The position of *F* corresponds to the boxed area in *E*. (*G*) Quantitation of Sox2$^+$ RGPs per 100-μm cortical column at E14.5, E16.5, and E18.5. Data are shown as mean ± SEM ***$P < 0.001$, Student's *t* test, $n = 6$ for E14.5 and E16.5, $n = 4$ for E18.5. (*H* and *J*) Diagram of coronal brain sections at E14.5 (*H*) and E16.5 (*J*), repectively. The *Right* in *H* and *J* are from boxed areas on the *Left*, respectively. (*I* and *K*) IPs are dramatically decreased in Nae1 CKO mice, as revealed by immunostaining of Tbr2 (a marker for IP) at E14.5 (*I*) and E16.5 (*K*). The position of *I* and *K* corresponds to the boxed area in *H* and *J*, respectively. (*L*) Quantitation of Tbr2$^+$ IPs per 100-μm cortical column at E14.5 and E16.5 by immunostaining. Data are shown as mean ± SEM ***$P < 0.001$, ****$P < 0.0001$, Student's *t* test, $n = 6$. (*M*) Diagram of RGP and IP proliferation and differentiation. (*N*) Diagram of cortex at E14.5 and E16.5. CP, cortical plate; IZ, intermediate zone. (*O* and *P*) PH3$^+$ mitotic cells are changed in VZ surface and non-VZ surface of Nae1 CKO mice at E14.5 and E16.5, shown by immunostaining. RGP proliferation is increased at E16.5 shown by VZ surface PH3$^+$ cells and IP proliferation is decreased at E14.5 shown by non-VZ surface PH3$^+$ cells. (*Q* and *R*) Quantitation of PH3$^+$ mitotic cells per 100-μm cortical column in VZ surface and non-VZ surface at E14.5 and E16.5. Data are shown as mean ± SEM *$P < 0.05$, **$P < 0.01$, Student's *t* test. $n = 6$ at E14.5. $n = 7$ for control and $n = 6$ for Nae1 CKO mice at E16.5. (*S*) Schematic diagram of BrdU pulse labeling. Mice were injected with BrdU (50 mg/kg body weight, i.p.) at E15.5 and killed at E16.5. (*T*) Double immunostaining of BrdU and Ki67 (cell cycle marker) shows the cell cycle exit is decreased in Nae1 CKO mice at E16.5, 24 h after BrdU injection. (*U*) Quantitation of ratio of BrdU$^+$Ki67$^+$ to total BrdU$^+$ cells at E16.5. Data are shown as mean ± SEM **$P < 0.01$, Student's *t* test, $n = 4$. (*V* and *W*) No apoptotic cells are observed at E14.5 in both control and Nae1 CKO mouse cortex, by immunostaining for cleaved Caspase-3 (an apoptotic marker). Diagrams of coronal brain sections of control and Nae1 CKO mice are shown. (*X* and *Y*) Cell apoptosis occurs at E16.5 in Nae1 CKO mice. Cleaved Caspase-3-positive cells show a dramatic increase at E16.5. Diagrams of coronal brain sections of control and Nae1 CKO mice are shown. (*Z*) Quantitation of cleaved Caspase-3$^+$ cells per 200-μm cortical column. Data are shown as mean ± SEM ***$P < 0.001$, Student's *t* test. At E14.5, $n = 3$ for control and $n = 4$ for Nae1 CKO mice. At E16.5, $n = 3$. (Scale bar, 100 μm in *B*, *D*, *F*, *I*, *K*, *O*, *P*, *T*, *V*, *W*, *X*, and *Y*.)

(19, 22), phenotypes similar to those in Nae1 CKO mice described above, supporting our initial hypothesis. We next determined whether this up-regulation of β-catenin level and signaling serve as a mechanism in cortical lamination of Nae1 CKO mice. We examined the expression pattern of β-catenin in developing cortex (Fig. 6*A*). Immunostaining for β-catenin at E16.5 showed increased nuclear intensity in progenitors (indicated by *) of the VZ (Fig. 6 *B*–*E*). Next, we used a Wnt/β-catenin signaling reporter mouse line, Axin2^{LacZ} mice (51), to determine whether β-catenin activity is altered in Nae1 CKO mice and generated Axin2$^{LacZ/+}$ and Nae1 CKO;Axin2$^{LacZ/+}$ mice. X-gal staining revealed high β-galactosidase activity in the VZ of Nae1 CKO;Axin2$^{LacZ/+}$ mice, but it was barely detectable in control Axin2$^{LacZ/+}$ mice (Fig. 6 *F* and *G*). Furthermore, Western blot analysis of cortical lysates from E15.5 embryos showed increased levels of active β-catenin, phosphorylated β-catenin (S33/S37), and total β-catenin in Nae1 CKO mice, compared with control mice (Fig. 6 *H* and *I*). Taken together, these data indicate Wnt/β-catenin signaling is elevated in the cortex of Nae1 CKO mice. Because activating Wnt/β-catenin signaling also increased Notch signaling (19), we determined whether Notch signaling was altered in Nae1 CKO mice. By in utero electroporating CBFRE-EGFP, a reporter of Notch signaling (52), into the VZ, we found that the number of high CBFRE-EGFP^{+} cells was increased in Nae1 CKO mice (*SI Appendix*, Fig. S7), suggesting Notch signaling is also increased in Nae1 CKO mice.

As mentioned above, Nae1 CKO mice displayed similar phenotypes—reduced IPs, enhanced apoptosis, and impaired lamination—to those of β-catenin gain-of-function mice which express a constitutively active β-catenin in the cortex (19, 22). These results are consistent with our conclusion that Nae1 knockout results

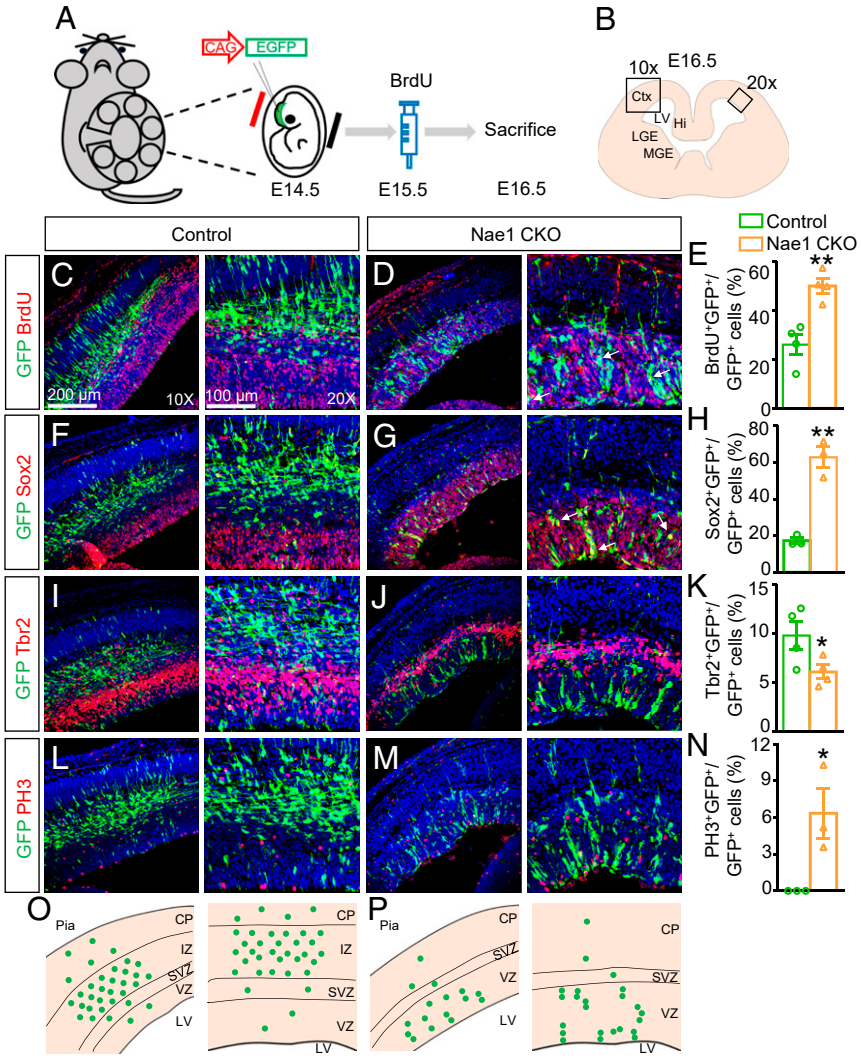

Fig. 5. Compromised differentiation of Nae1-deficient progenitor cells. (*A*) Schematic diagram of IUE and following BrdU injection and mouse killing at designated time points. Embryos were transfected with CAG-EGFP plasmids at E14.5. BrdU (50 mg/kg body weight, i.p.) was injected at E15.5 and pregnant mice were killed at E16.5. (*B*) Diagrams of coronal brain sections at E16.5. The large boxed area (10×) corresponds to the *Left* in *C*, *D*, *F*, *G*, *I*, *J*, *L*, and *M*. The small boxed area (20×) corresponds to the *Right* in *C*, *D*, *F*, *G*, *I*, *J*, *L*, and *M*. Ctx, cortex; LV, lateral ventricle; Hi, hippocampus; LGE, lateral ganglionic eminence; MGE, medial ganglionic eminence. (*C*–*E*) More GFP^{+} cells are in proliferation because more are labeled with BrdU by immunostaining in Nae1 CKO mice, as shown by a higher ratio of BrdU^{+}/GFP^{+} to total GFP^{+} cells. (*F*–*H*) More GFP^{+} cells are RGPs in Nae1 CKO mice because of a higher ratio of Sox2^{+}/GFP^{+} to total GFP^{+} cells by immunostaining of Sox2. (*I*–*K*) Fewer GFP^{+} cells are IP cells in Nae1 CKO mice due to a lower ratio of Tbr2^{+}/GFP^{+} to total GFP^{+} cells by immunostaining of Tbr2. (*L*–*N*) More GFP^{+} cells are mitotic in Nae1 CKO mice, as revealed by a higher ratio of PH3^{+}/GFP^{+} to total GFP^{+} cells via immunostaining of PH3. (*O* and *P*) Schematic diagram showing the distribution of GFP-transfected cells in control and Nae1 CKO mice. Green dots represent GFP^{+} cells. Pia, pial surface; CP, cortical plate; IZ, intermediate zone; SVZ, subventricular zone; VZ, ventricular zone (Scale bars, 200 μm in *Left* and 100 μm in *Right* in *C*, *D*, *F*, *G*, *I*, *J*, *L*, and *M*.) Data are shown as mean ± SEM *$P < 0.05$, **$P < 0.01$, Student's *t* test, $n = 4$ for *E* and *K* and $n = 3$ for *H* and *N*.

in elevated Wnt/β-catenin signaling in cortical progenitors. To test this hypothesis, we determined whether knockdown of β-catenin could rescue deficits of Nae1 CKO mice. A shRNA against β-catenin was constructed as previously reported (53). Its efficacy to knock down β-catenin was validated by Western blots with β-catenin antibody in HEK293T cells cotransfected with β-catenin and shRNA (Fig. 6*J*). Next, the shRNA together with CAG-EGFP plasmids were introduced into embryonic cortex at E14.5 by IUE. Mice were injected 24 h later with BrdU and killed at E16.5 (Fig. 6*K*). Cortical slices were double immunostained for BrdU and Sox2 to examine the proliferation and the progenitor state of GFP-labeled cells (Fig. 6 *L* and *M*). A subpopulation of cells with shRNA migrated out of BrdU- or Sox2-stained zones, but fewer cells were costained with BrdU or Sox2 in Nae CKO mice (Fig. 6 *N*–*S*), unlike those cells with GFP only in Nae1 CKO mice (Fig. 5 *C*–*H*). These results indicate a partial rescue from Nae1 deletion by suppressing β-catenin. Taken together, these observations support a working model that downregulation of β-catenin serves as a mechanism to drive them out of the progenitor state in Nae1 mutant mice.

Discussion

Our study provides evidence for an indispensable role of neddylation in the development of the cortex and hippocampus. We showed that neddylation is necessary for the proliferation and differentiation of the cortical progenitors and promotes their survival. When neddylation is blocked by Nae1 CKO, RGPs are overproduced at E16.5, but become apoptotic and reduced at E18.5; consequently, the generation of IPs and neurons become

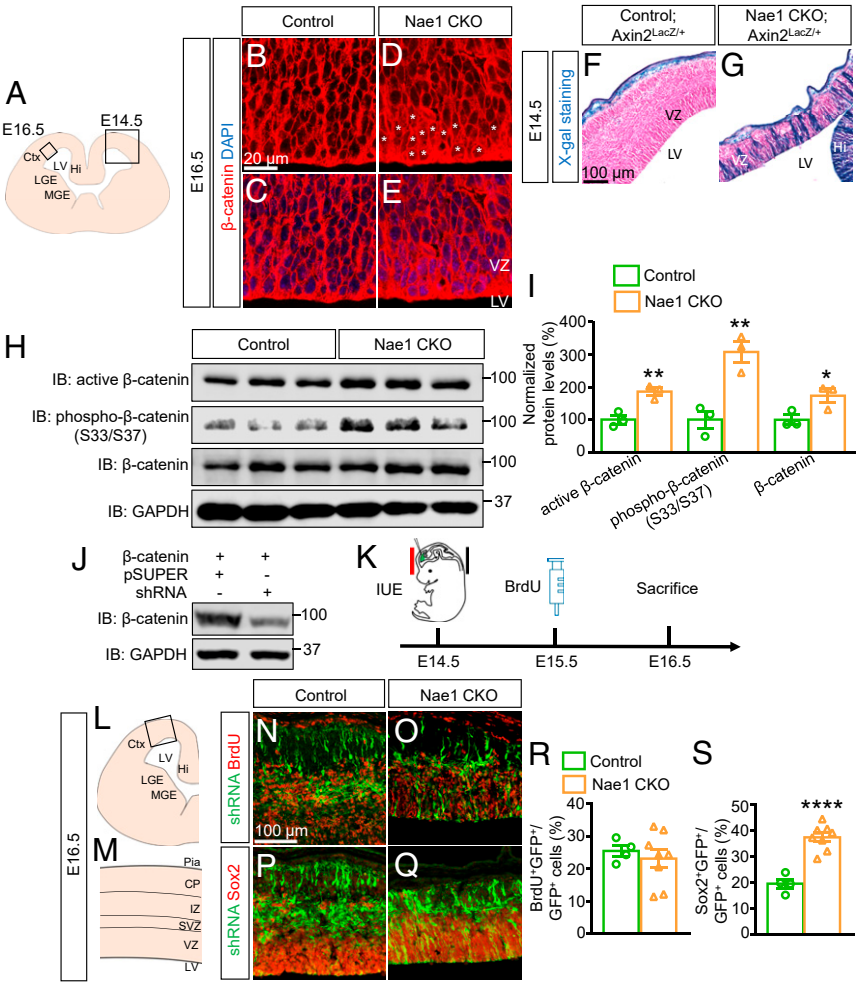

Fig. 6. Increased β-catenin signaling in Nae1 CKO mice. (A) Diagram of a coronal brain section in a mouse embryo. The *Left* boxed area corresponds to *B*–*E* and the *Right* boxed area corresponds to *F* and *G*. Ctx, cortex; LV, lateral ventricle; Hi, hippocampus; LGE, lateral ganglionic eminence; MGE, medial ganglionic eminence. (*B*–*E*) β-Catenin is increased in VZ cell nuclei of Nae1 CKO mice at E16.5. Brain sections are immunostained with anti-β-catenin antibody and cell nuclei are counterstained with DAPI. Stars indicate increase of β-catenin fluorescence in nuclei. VZ, ventricular zone (Scale bar, 20 μm.) (*F* and *G*) β-Catenin signaling is increased in the VZ of Nae1 CKO mice at E14.5, as shown by Axin2$^{LacZ/+}$ reporter activity. Control and Nae1 CKO mice are crossed with Axin2$^{LacZ/+}$ reporter line and β-galactosidase activity is revealed by X-gal staining (Scale bar, 100 μm.) (*H* and *I*) Active β-catenin, phospho-β-catenin (S33/S37), and total β-catenin are increased in Nae1 CKO mice at E15.5, as shown by Western blots. For quantitation, data are normalized and shown as mean ± SEM $*P < 0.05$, $**P < 0.01$, Student's *t* test, $n = 3$. (*J*) β-Catenin is decreased in HEK293T cells transfected with shRNA of β-catenin. Cells are transfected with β-catenin expression plasmid with pSUPER control or β-catenin shRNA, and β-catenin protein level was determined by Western blots. (*K*) Schematic diagram of IUE, BrdU injection, and mouse killing from E14.5 to E16.5. (*L* and *M*) Diagram of coronal brain section at E16.5. The *M* is from the boxed area in *L* and corresponds to *N*–*Q*. Pia, pial surface; CP, cortical plate; IZ, intermediate zone; SVZ, subventricular zone. (*N*–*Q*) Fewer GFP$^+$ cells (with β-catenin knockdown) are in proliferation or RGPs. Brain sections from control and Nae1 CKO mice with IUE and BrdU injection are immunostained with BrdU and Sox2 antibodies. The ratio of BrdU$^+$/GFP$^+$ to total GFP$^+$ cells is comparable between control and Nae1 CKO mice and the ratio of Sox2$^+$/GFP$^+$ to total GFP$^+$ cells is around 40%. Both ratios are reduced, as compared with Fig. 3 *E* and *H*. (Scale bar, 100 μm.) (*R* and *S*) Quantitation of ratios of BrdU$^+$/GFP$^+$ to total GFP$^+$ cells and Sox2$^+$/GFP$^+$ to total GFP$^+$ cells. Data are shown as mean ± SEM $****P < 0.0001$, Student's *t* test. $n = 4$ for control and $n = 8$ for Nae1 CKO mice.

problematic, leading to a reduction in cortical neurons. In addition, Nae1 mutation diminished the number of Reelin$^+$ and Calretinin$^+$ cells in layer I, which are known to be critical for new-born neurons to populate the cortex (54). Moreover, RGPs are reduced, which were unable to provide sufficient radial fiber scaffolds for neuron migration. Consequently, the cortex of Nae1 CKO mice is disorganized.

Wnt/β-catenin signaling drives the neural stem and progenitor cells' self-renewal, proliferation, and expansion during embryonic cortical development (55). Overexpression of Wnt3a in cortical progenitors promotes RGP self-renewal (56). Expression of activated β-catenin in developing brain leads to expansion of cortical progenitor pool and increase of apoptosis (21, 57). Overexpression of a constitutively active β-catenin in mice reveals enlarged ventricles, reduced IPs, and an initial expansion of Pax6$^+$ VZ with a subsequent loss, probably due to elevated apoptosis (19, 22). Thus, these results support the notion that Wnt/β-catenin signaling maintains the progenitor proliferation in cortical development. The phenotypes we discovered in the current study are similar to those of β-catenin gain-of-function mice: 1) RGPs are promoted initially but declined later (Fig. 4), 2) IPs and neurons are decreased (Figs. 2 and 4), 3) cell apoptosis is elevated (Fig. 4 and *SI Appendix*, Fig. S6), and 4) cortex is disorganized and lamination is defective (Fig. 2) (19, 22, 57). Of note, the phenotypes in Nae1 CKO mice appeared to be milder than those in transgenic mice overexpressing activated β-catenin (21). This may be due to the fact the transgene is overexpressed on top of the endogenous β-catenin in transgenic mice, and every molecule of the transgene is "activated β-catenin." However, in our study, we mutated Nae1, which stabilized endogenous β-catenin protein and caused eventual increase in activated β-catenin by only two folds (Fig. 6 *H* and *I*). In addition to β-catenin, Notch signaling was increased in the VZ of Nae1 CKO mice (*SI Appendix*, Fig. S7). Further studies will be necessary to determine the contribution of increased Notch signaling to the observed phenotypes.

We demonstrate here that β-catenin is regulated by neddylation. First, β-catenin level is increased in MLN-4924-treated cells and Nae1 CKO mouse cortex (*SI Appendix*, Fig. S1*A* and Fig. 6 *H* and *I*) and in nuclei of mutant VZ (Fig. 6 *A*–*E*). Second, Wnt/β-catenin signaling is increased in MLN-4924-treated cells and Nae1 CKO mouse cortex (*SI Appendix*, Fig. S1*B* and Fig. 6 *F* and *G*). Third, β-catenin can be neddylated (Fig. 1 *A*–*D*). Prevention of β-catenin neddylation by K170R and K233R increased nuclear localization (Fig. 1 *F*–*M*). Finally, suppressing β-catenin in Nae1 CKO mouse cortex rescues the overproliferation of mutant cortical progenitors (Fig. 6 *N*–*S*). These observations suggest a role of neddylation in regulating β-catenin level. The β-catenin protein is composed of a N-terminal domain, a central region with 12 armadillo repeats, and a C-terminal domain (58). Previous studies suggest that β-catenin interaction partners TCF4 and BCL9 recruit β-catenin to the nucleus, while APC and Axin enrich β-catenin in the cytoplasm, by retaining it in the compartment where they are localized (59). The armadillo repeats R1 to R9 of β-catenin serve as a core binding site for these interaction partners (58). Although five lysine residues (K19, K170, K233, K354, and K625) could be neddylated (Fig. 1*E*), only K170 and K233 increased nuclear localization (with K354 showing a trend without statistic difference) (Fig. 1 *F*–*M*). Noticeably, three residues are localized in R1 to R9 whereas K19 and K625 are not. Thus, it is possible that mutations of K170, K233, and K354 disrupt the interaction between β-catenin and one or more of these binding partners, causing an increase of nuclear localization of β-catenin. The functional consequence of neddylation at K19 and K625 warrants future studies.

Wnt/β-catenin signaling is critical not only to cortical development, but also to that of the hippocampus. In Wnt3a knockout mice, the hippocampus is small or missing, as a result of reduced cell proliferation (60). On the other hand, in mice expressing a constitutively active β-catenin, the hippocampus is not detected either (22). In our study, because Emx1-Cre is active in cerebral cortex as well as hippocampus (36), Nae1 is deleted in both brain regions early in development. An apparent phenotype for postnatal Nae1 CKO brain is loss of most hippocampal structure (Fig. 2*E* and *SI Appendix*, Fig. S3*E*) and remaining hippocampus became extremely small but remained connected with medial cortex. The more severe phenotypes in the hippocampus than the cortex may be because the development of the cortex occurs prior to that of the hippocampus. Emx1-Cre is expressed in the progenitor cells for the cortex and hippocampus at the same time (i.e., E12.5) (36). At this time, new-born neurons have begun migrating to populate the cortex, perhaps having escaped the effect of Nae1 mutation on apoptosis. However, only around E14, hippocampal neurons are beginning to be generated from progenitors.

Materials and Methods

Mice. Nae1$^{f/f}$ mice (26) were crossed with Emx1-Cre mice (027784; The Jackson Laboratory) to obtain Emx1-Cre;Nae1$^{f/f}$ (referred to as Nae1 CKO) mice, in which Nae1 was specifically deleted in cerebral cortex and hippocampus since E10.5 (36). Wnt/β-catenin signaling reporter Axin2$^{LacZ/+}$ mice (009120; The Jackson Laboratory) were also crossed with Emx1-Nae1$^{+/-}$ to generate Nae1 CKO;Axin2$^{LacZ/+}$ mice, to visualize Wnt/β-catenin signaling activity by X-gal staining. Genotyping was done as previously reported (27) or according to The Jackson Laboratory's protocols. Littermates with genotypes of Nae1$^{f/f}$ or Nae1$^{f/+}$ were used as controls. All animal manipulations and experiments were approved by the Institutional Animal Care and Use Committee of Case Western Reserve University.

Plasmids. CAG-EGFP (50), HA-Nedd8, HA-Nedd8ΔGG, and myc-Nedp1 were used as previously reported (61). CBFRE-EGFP was a gift from Nicholas Gaiano, National Institute of Mental Health, Bethesda, MD (Addgene plasmid 17705) (62). Flag-β-catenin was generated by cloning mouse full-length β-catenin coding sequence into pCAGGS vector with a Flag tag in the N terminus. Flag-β-catenin constructs containing site mutations (K19R, K133R, K158R, K170R, K233R, K335R, K354R, K435R, and K625R) were generated by site-directed mutagenesis with inverse PCR. The shRNA of β-catenin was targeted against 5′-CTGAT ATTGA CGGGC AGTAT-3′ as reported previously (53). The oligonucleotides were annealed and then inserted into the pSUPER vector. The empty pSUPER vector served as a control.

In Utero Electroporation. The in utero electroporation was performed as previously described (50). Briefly, a pregnant mouse was deeply anesthetized by isoflurane or ketamine/xylazine and its uterus was exposed and kept moist by saline during the whole procedure. Approximately 0.5 μL plasmid with 0.01% Fast Green was injected into the lateral ventricle of embryos through a capillary. The injected plasmids included CAG-EGFP only (1 μg/μL), β-catenin-shRNA+CAG-EGFP (1 μg/μL for each), or CBFRE-EGFP only (1 μg/μL). Five electric pulses of 36 V with 50-ms duration and 950-ms interval were delivered to the embryo brain by a pair of tweezer-like electrodes, connected with an electroporator (ECM830, BTX). When the abdomen was sutured, the mouse was put on a heated pad until it woke up from anesthesia. One or 2 d after surgery, the mouse was killed, and the embryo were dissected out for experiments.

Transient Transfection. HEK293T cells were maintained in Dulbecco's Modified Eagle Medium (DMEM; Corning) containing 10% fetal bovine serum (FBS; HyClone). When confluence reached 80%, cells were digested in 0.05% trypsin (Gibco) and passaged at a 1:4 ratio. For transient transfection, cells were passaged 1 d before and transfected using polyethyleneimine (PEI, 1 mg/mL, molecular weight 25,000) (23966-1, Polysciences). The ratio of DNA to PEI was 1:3. For drug treatment, cells were treated with MLN-4924 (2 μM; Active Biochem) or vehicle (dimethyl sulfoxide, DMSO; Sigma) for 12 h. Cells were then collected and washed in ice-cold phosphate-buffered saline (PBS) and cell pellet was resuspended in hypotonic buffer (20 mM Tris·HCl pH 7.4, 10 mM NaCl, 3 mM $MgCl_2$) with protease and phosphatase inhibitor mixture tablets (Roche) for 15 min on ice. Nonidet P-40 was then added and the homogenates were centrifuged for 10 min at 3,000 rpm at 4 °C. The supernatant contained the cytoplasmic fraction. The pellet that contained the nuclear fraction was lysed in cell extraction buffer (10 mM Tris·HCl pH 7.4, 100 mM NaCl, 1% Triton X-100, 0.5% sodium deoxycholate, 0.1% SDS, 1 mM

ethylenediaminetetraacetic acid [EDTA]) and further cleared by spinning for 30 min at 14,000 × *g* at 4 °C. The cytoplasmic and nuclear fractions were analyzed by Western blotting.

Protein Stability Assay. CHX (10 μg/mL; C1988, Sigma) was used to inhibit protein synthesis in HEK293T cells. Cells were treated with CHX+vehicle or CHX+MLN-4924 (2 μM) for 1, 2, 4, 6, 12, 18, or 24 h. Total proteins were extracted using RIPA buffer (50 mM Tris·HCl pH 7.4, 150 mM NaCl, 1% Nonidet P-40, 0.5% sodium deoxycholate, 0.1% SDS, 5 mM EDTA) supplemented with protease and phosphatase inhibitor mixtures (Roche). Samples were analyzed by Western blotting.

Luciferase Assay. Cells were transfected with TOPFlash and pRL-TK vectors (DNA ratio 10:1). The TOPFlash reporter contained TCF binding sites and the firefly luciferase gene, which was expressed when Wnt/β-catenin signaling was activated. The pRL-TK contained the Renilla luciferase gene, which constitutively expressed and served as an internal control. After 24 h posttransfection, cells were treated with MLN-4924 (2 μM) or vehicle for 12 h. Luciferase activities were measured using the Dual-Glo luciferase assay system (Promega) according to the manufacturer's instruction. For measurement of luciferase activity, the firefly luminescence of the cells was normalized to the Renilla luminescence and this ratio from MLN-4924-treated cells was then normalized to that from vehicle-treated cells.

Coprecipitation and Western Blotting. HEK293T cells and mouse cortical tissues were lysed in RIPA buffer (50 mM Tris·HCl pH 7.4, 150 mM NaCl, 1% Nonidet P-40, 0.5% sodium deoxycholate, 0.1% SDS, 5 mM EDTA) supplemented with a protease inhibitor mixture (Roche). Protein concentration was determined using the bicinchoninic acid (BCA) method (Thermo Scientific). The lysate was used immediately or incubated with Anti-FLAG M2 Affinity Gel (A2220, Sigma) or β-catenin antibody (C7207, Sigma) followed by Protein A/G PLUS-Agarose (sc-2003, Santa Cruz) at 4 °C overnight. Precipitated proteins were examined by Western blotting.

Equivalent mounts of protein samples were loaded for SDS-polyacrylamide gel electrophoresis with a molecular weight marker (Bio-Rad). Then the proteins on the gel were electrotransferred to nitrocellulose membrane (Bio-Rad). The membrane was incubated at 4 °C overnight with the following primary antibodies: Nae1 (1:500; No. 14321, Cell Signaling Technology), Nedd8 (1:250; No. 2745, Cell Signaling Technology), Cullin1 (1:500; sc-17775, Santa Cruz), GAPDH (1:500; sc-32233, Santa Cruz), β-catenin (1:1,000; C7207, Sigma), active β-catenin (1:1,000; No. 8814, Cell Signaling Technology), phospho-β-catenin (S33/S37) (1:1,000; C4231, Sigma), PARP (1:1,000; No. 9532, Cell Signaling Technology), α-tubulin (1:1,000; No. 2144, Cell Signaling Technology), Flag (1:1,000; F1804, Sigma), Myc (1:1,000; No. 2278, Cell Signaling Technology), p53 (1:1,000; No. 2524, Cell Signaling Technology) followed by incubation with species-specific HRP-conjugated secondary antibodies (1:5,000; Cell Signaling Technology) at room temperature for 1 h. The samples were visualized by enhanced chemiluminescence. ImageJ software was used to measure the band intensity and all data were normalized to those of internal controls.

Histochemical Characterizations. HEK293T cells were washed in PBS and fixed with 4% paraformaldehyde (PFA; Sigma) for 10 min. Cells were blocked in 10% bovine serum albumin (BSA)/PBS and incubated with anti-Flag (1:1,000; F1804, Sigma) antibody. Cells were then incubated with Alexa Fluor 594-conjugated mouse secondary antibodies (1:500, Jackson ImmunoResearch) and DAPI (Sigma) for counterstaining. For Flag immunoactivity in cells, the intensity of Flag fluorescence in the cell nuclei was measured and normalized to that in the cell cytoplasm.

Embryos older than E15.5 and postnatal mice were first perfused and fixed with 4% PFA at 4 °C overnight. Embryos younger than E15.5 underwent fixation directly without perfusion. After cryoprotective incubation (in 20% sucrose solution for embryos, 30% for postnatal brains), tissues were cut into 12- to 20-μm sections using a cryostat (NX70, Thermo Scientific). After treatment with 10 mM sodium citrate (pH 6.0) at 95 °C, sections were incubated at 4 °C overnight with the following primary antibodies: NeuN (1:500; MAB377, Millipore), GFAP (1:500; AB5804, Millipore), AldoC (1:500; sc-12065, Santa Cruz), Sox2 (1:200; MA1-014, Thermo Scientific), Tbr2 (1:500; ab23345, Abcam), PH3 (1:200; sc-374669, Santa Cruz), Ki67 (1:200; AB9260, Millipore), GFP (1:1,000; A-11122, Invitrogen), Ctip2 (1:500; ab18465, Abcam), Tuj1 (1:500; T8660, Sigma), Cux1 (1:200; M222, Santa Cruz), γH2AX (1:500; No. 9718, Cell Signaling Technology), cleaved Caspase-3 (1:100; No. 9661, Cell Signaling Technology), β-catenin (1:4,000; C7207, Sigma), Calretinin (1:2,000; No. 6B3, Swant), and phos-Vimentin (1:500; ab22651, abcam). Brain tissues were incubated with fluoro-conjugated species-specific secondary antibodies (1:500; Jackson ImmunoResearch) and DAPI for counterstaining. For cell counts of Ctip2, NeuN, AldoC, GFAP, Sox2, Tbr2, cleaved Caspase-3, γH2AX-positve cells in the cortical plate or cortex, all positive cells in a 100- or 200-μm-wide cortical columns from white matter to pial surface were counted. For the Tuj1-positive fluorescent area, the area with Tuj1$^+$ fluorescence was measured. For cell counts of Cux1$^+$ cells, only positive cells in cortical plate were counted, excluding those beneath the deeper cortical plate. For cell counts of PH3$^+$ cells, positive cells along the VZ surface or in non-VZ surface regions were quantified separately. For cleavage plane orientation of mitotic RGPs at anaphase/telophase at VZ surface, the angle between the cleavage plane and VZ surface was defined and measured. For cell counts of CBFRE-EGFP$^+$ cells, only high EGFP$^+$ cells in a 100-μm-wide cortical column were counted.

For BrdU labeling, one pulse of BrdU (50 mg/kg body weight, i.p.) was administered to pregnant mice. One hour or 24 h later, mice were killed, and brains were sectioned as mentioned above. Before incubation with BrdU (1:500; ab6326, Abcam) and/or primary antibodies (Sox2, Ki67, or GFP), brain slices were treated with 0.01 M sodium citrate at 95 °C for 5 min, 2 N HCl for 20 min at 37 °C, 0.1 M borate buffer (pH 8.5) for 10 min at room temperature. For cell counts of BrdU/Ki67, BrdU/GFP, Sox2/GFP, Tbr2/GFP, PH3/GFP, BrdU/shRNA(GFP), or Sox2/shRNA(GFP) colocalization, all double-positive and GFP-positive cells in the same field were counted and the ratio of double-positive cells to GFP-positive cells was calculated.

For in situ hybridization, the full coding sequence of Nae1 was used as the template for antisense probe. Sense probe of Nae1 was used as a negative control. Reelin probe was used as previously reported (63). Before incubation with RNA probes (antisense or sense) at 65 °C overnight, brain sections were sequentially digested by proteinase K, fixed in 4% PFA, treated with triethanolamine/acetic anhydride and blocked in prehybridization buffer (50% formamide, 5× saline sodium citrate [SSC], 0.3 mg/mL yeast tRNA, 100 μg/mL heparin, 1× Denhardt's solution, 0.1% Tween-20, 0.1% CHAPS, 5 mM EDTA). Then the slices were washed and incubated with anti-Digoxigenin-AP antibody (Roche) at 4 °C overnight. Finally, the mRNA signal was visualized by NBT (nitro-blue tetrazolium chloride) and BCIP (5-bromo-4-chloro-3′-indolyphosphate p-toluidine salt) incubation.

For Nissl staining, brain sections were incubated in cresyl violet solution (FD NeuroTechnologies) for 1 min, then dehydrated in ethanol, cleared in xylene, and mounted with DPX Mountant (Sigma). For measurement of cortical thickness, the dorsolateral cortex at the same level was chosen and measured with ImageJ.

For X-gal staining, embryos were dissected out and fixed in 4% PFA for 20 min. After cutting, brain sections were washed in PBS and incubated with X-gal staining solution [1 mg/mL X-gal, 5 mM $K_3Fe(CN)_6$, 5 mM $K_4Fe(CN)_6$, 2 mM $MgCl_2$ in PBS] at 37 °C overnight. Following several washes in PBS, brain sections were counterstained with Fast Red (Vector Labs).

Statistics. Comparison was performed using Student's *t* test or one-way ANOVA with post hoc Dunnett's test. The *P* value of less than 0.05 was considered significant. All data were presented as mean ± SEM.

Data Availability. All study data are included in the article text and *SI Appendix*.

ACKNOWLEDGMENTS. We thank all the members of the L.M. and W.-C.X. laboratories for helpful discussions.

1. B. J. Molyneaux, P. Arlotta, J. R. Menezes, J. D. Macklis, Neuronal subtype specification in the cerebral cortex. *Nat. Rev. Neurosci.* **8**, 427–437 (2007).
2. L. C. Greig, M. B. Woodworth, M. J. Galazo, H. Padmanabhan, J. D. Macklis, Molecular logic of neocortical projection neuron specification, development and diversity. *Nat. Rev. Neurosci.* **14**, 755–769 (2013).
3. W. Haubensak, A. Attardo, W. Denk, W. B. Huttner, Neurons arise in the basal neuroepithelium of the early mammalian telencephalon: A major site of neurogenesis. *Proc. Natl. Acad. Sci. U.S.A.* **101**, 3196–3201 (2004).
4. S. C. Noctor, V. Martínez-Cerdeño, A. R. Kriegstein, Contribution of intermediate progenitor cells to cortical histogenesis. *Arch. Neurol.* **64**, 639–642 (2007).
5. A. Pontious, T. Kowalczyk, C. Englund, R. F. Hevner, Role of intermediate progenitor cells in cerebral cortex development. *Dev. Neurosci.* **30**, 24–32 (2008).
6. D. V. Hansen, J. H. Lui, P. R. Parker, A. R. Kriegstein, Neurogenic radial glia in the outer subventricular zone of human neocortex. *Nature* **464**, 554–561 (2010).
7. X. Wang, J. W. Tsai, B. LaMonica, A. R. Kriegstein, A new subtype of progenitor cell in the mouse embryonic neocortex. *Nat. Neurosci.* **14**, 555–561 (2011).
8. S. C. Noctor, V. Martínez-Cerdeño, L. Ivic, A. R. Kriegstein, Cortical neurons arise in symmetric and asymmetric division zones and migrate through specific phases. *Nat. Neurosci.* **7**, 136–144 (2004).
9. T. Miyata, A. Kawaguchi, H. Okano, M. Ogawa, Asymmetric inheritance of radial glial fibers by cortical neurons. *Neuron* **31**, 727–741 (2001).

10. S. C. Noctor, A. C. Flint, T. A. Weissman, R. S. Dammerman, A. R. Kriegstein, Neurons derived from radial glial cells establish radial units in neocortex. *Nature* **409**, 714–720 (2001).
11. P. Rakic, Guidance of neurons migrating to the fetal monkey neocortex. *Brain Res.* **33**, 471–476 (1971).
12. C. G. Silva, E. Peyre, L. Nguyen, Cell migration promotes dynamic cellular interactions to control cerebral cortex morphogenesis. *Nat. Rev. Neurosci.* **20**, 318–329 (2019).
13. B. Martynoga, D. Drechsel, F. Guillemot, Molecular control of neurogenesis: A view from the mammalian cerebral cortex. *Cold Spring Harb. Perspect. Biol.* **4**, a008359 (2012).
14. Z. Steinhart, S. Angers, Wnt signaling in development and tissue homeostasis. *Development* **145**, dev146589 (2018).
15. S. Angers, R. T. Moon, Proximal events in Wnt signal transduction. *Nat. Rev. Mol. Cell Biol.* **10**, 468–477 (2009).
16. C. A. Mutch, N. Funatsu, E. S. Monuki, A. Chenn, Beta-catenin signaling levels in progenitors influence the laminar cell fates of projection neurons. *J. Neurosci.* **29**, 13710–13719 (2009).
17. I. Vitali *et al*., Progenitor hyperpolarization regulates the sequential generation of neuronal subtypes in the developing neocortex. *Cell* **174**, 1264–1276.e15 (2018).
18. O. Machon, C. J. van den Bout, M. Backman, R. Kemler, S. Krauss, Role of beta-catenin in the developing cortical and hippocampal neuroepithelium. *Neuroscience* **122**, 129–143 (2003).
19. N. Nakagawa *et al*., APC sets the Wnt tone necessary for cerebral cortical progenitor development. *Genes Dev.* **31**, 1679–1692 (2017).
20. K. Draganova *et al*., Wnt/β-catenin signaling regulates sequential fate decisions of murine cortical precursor cells. *Stem Cells* **33**, 170–182 (2015).
21. A. Chenn, C. A. Walsh, Regulation of cerebral cortical size by control of cell cycle exit in neural precursors. *Science* **297**, 365–369 (2002).
22. J. Pöschl, D. Grammel, M. M. Dorostkar, H. A. Kretzschmar, U. Schüller, Constitutive activation of β-catenin in neural progenitors results in disrupted proliferation and migration of neurons within the central nervous system. *Dev. Biol.* **374**, 319–332 (2013).
23. S. Kandala, I. M. Kim, H. Su, Neddylation and deneddylation in cardiac biology. *Am. J. Cardiovasc. Dis.* **4**, 140–158 (2014).
24. R. I. Enchev, B. A. Schulman, M. Peter, Protein neddylation: Beyond cullin-RING ligases. *Nat. Rev. Mol. Cell Biol.* **16**, 30–44 (2015).
25. H. S. Park *et al*., PPARγ neddylation essential for adipogenesis is a potential target for treating obesity. *Cell Death Differ.* **23**, 1296–1311 (2016).
26. J. Zou *et al*., Neddylation mediates ventricular chamber maturation through repression of Hippo signaling. *Proc. Natl. Acad. Sci. U.S.A.* **115**, E4101–E4110 (2018).
27. A. M. Vogl *et al*., Neddylation inhibition impairs spine development, destabilizes synapses and deteriorates cognition. *Nat. Neurosci.* **18**, 239–251 (2015).
28. L. Li *et al*., Enzymatic activity of the scaffold protein Rapsyn for synapse formation. *Neuron* **92**, 1007–1019 (2016).
29. A. M. Vogl *et al*., Global site-specific neddylation profiling reveals that NEDDylated cofilin regulates actin dynamics. *Nat. Struct. Mol. Biol.* **27**, 210–220 (2020).
30. T. A. Soucy *et al*., An inhibitor of NEDD8-activating enzyme as a new approach to treat cancer. *Nature* **458**, 732–736 (2009).
31. A. Sarikas, T. Hartmann, Z. Q. Pan, The cullin protein family. *Genome Biol.* **12**, 220 (2011).
32. H. Walden *et al*., The structure of the APPBP1-UBA3-NEDD8-ATP complex reveals the basis for selective ubiquitin-like protein activation by an E1. *Mol. Cell* **12**, 1427–1437 (2003).
33. H. M. Mendoza *et al*., NEDP1, a highly conserved cysteine protease that deNEDDylates Cullins. *J. Biol. Chem.* **278**, 25637–25643 (2003).
34. K. E. Coleman *et al*., SENP8 limits aberrant neddylation of NEDD8 pathway components to promote cullin-RING ubiquitin ligase function. *eLife* **6**, e24325 (2017).
35. N. Chow, J. R. Korenberg, X. N. Chen, R. L. Neve, APP-BP1, a novel protein that binds to the carboxyl-terminal region of the amyloid precursor protein. *J. Biol. Chem.* **271**, 11339–11346 (1996).
36. J. A. Gorski *et al*., Cortical excitatory neurons and glia, but not GABAergic neurons, are produced in the Emx1-expressing lineage. *J. Neurosci.* **22**, 6309–6314 (2002).
37. M. K. Lee, J. B. Tuttle, L. I. Rebhun, D. W. Cleveland, A. Frankfurter, The expression and posttranslational modification of a neuron-specific beta-tubulin isotype during chick embryogenesis. *Cell Motil. Cytoskeleton* **17**, 118–132 (1990).
38. P. Arlotta *et al*., Neuronal subtype-specific genes that control corticospinal motor neuron development in vivo. *Neuron* **45**, 207–221 (2005).
39. M. Nieto *et al*., Expression of Cux-1 and Cux-2 in the subventricular zone and upper layers II-IV of the cerebral cortex. *J. Comp. Neurol.* **479**, 168–180 (2004).
40. S. Lodato, P. Arlotta, Generating neuronal diversity in the mammalian cerebral cortex. *Annu. Rev. Cell Dev. Biol.* **31**, 699–720 (2015).
41. C. C. Homem, M. Repic, J. A. Knoblich, Proliferation control in neural stem and progenitor cells. *Nat. Rev. Neurosci.* **16**, 647–659 (2015).
42. C. Dehay, H. Kennedy, Cell-cycle control and cortical development. *Nat. Rev. Neurosci.* **8**, 438–450 (2007).
43. D. Y. Zhang, H. J. Wang, Y. Z. Tan, Wnt/β-catenin signaling induces the aging of mesenchymal stem cells through the DNA damage response and the p53/p21 pathway. *PLoS One* **6**, e21397 (2011).
44. S. Tao *et al*., Wnt activity and basal niche position sensitize intestinal stem and progenitor cells to DNA damage. *EMBO J.* **34**, 624–640 (2015).
45. W. P. Roos, B. Kaina, DNA damage-induced cell death by apoptosis. *Trends Mol. Med.* **12**, 440–450 (2006).
46. Z. F. Zimmerman, R. M. Kulikauskas, K. Bomsztyk, R. T. Moon, A. J. Chien, Activation of Wnt/β-catenin signaling increases apoptosis in melanoma cells treated with trail. *PLoS One* **8**, e69593 (2013).
47. M. Ming *et al*., Activation of Wnt/β-catenin protein signaling induces mitochondria-mediated apoptosis in hematopoietic progenitor cells. *J. Biol. Chem.* **287**, 22683–22690 (2012).
48. J. S. Brown, S. P. Jackson, Ubiquitylation, neddylation and the DNA damage response. *Open Biol.* **5**, 150018 (2015).
49. K. H. Vousden, D. P. Lane, p53 in health and disease. *Nat. Rev. Mol. Cell Biol.* **8**, 275–283 (2007).
50. L. Zhang *et al*., Satb2 is required for dendritic arborization and soma spacing in mouse cerebral cortex. *Cereb. Cortex* **22**, 1510–1519 (2012).
51. B. Lustig *et al*., Negative feedback loop of Wnt signaling through upregulation of conductin/axin2 in colorectal and liver tumors. *Mol. Cell. Biol.* **22**, 1184–1193 (2002).
52. Y. Xie, C. Jüschke, C. Esk, S. Hirotsune, J. A. Knoblich, The phosphatase PP4c controls spindle orientation to maintain proliferative symmetric divisions in the developing neocortex. *Neuron* **79**, 254–265 (2013).
53. Y. Mao *et al*., Disrupted in schizophrenia 1 regulates neuronal progenitor proliferation via modulation of GSK3beta/beta-catenin signaling. *Cell* **136**, 1017–1031 (2009).
54. D. S. Rice, T. Curran, Role of the reelin signaling pathway in central nervous system development. *Annu. Rev. Neurosci.* **24**, 1005–1039 (2001).
55. N. Bengoa-Vergniory, R. M. Kypta, Canonical and noncanonical Wnt signaling in neural stem/progenitor cells. *Cell. Mol. Life Sci.* **72**, 4157–4172 (2015).
56. R. N. Munji, Y. Choe, G. Li, J. A. Siegenthaler, S. J. Pleasure, Wnt signaling regulates neuronal differentiation of cortical intermediate progenitors. *J. Neurosci.* **31**, 1676–1687 (2011).
57. D. Zechner *et al*., beta-Catenin signals regulate cell growth and the balance between progenitor cell expansion and differentiation in the nervous system. *Dev. Biol.* **258**, 406–418 (2003).
58. T. Valenta, G. Hausmann, K. Basler, The many faces and functions of β-catenin. *EMBO J.* **31**, 2714–2736 (2012).
59. E. Krieghoff, J. Behrens, B. Mayr, Nucleo-cytoplasmic distribution of beta-catenin is regulated by retention. *J. Cell Sci.* **119**, 1453–1463 (2006).
60. S. M. Lee, S. Tole, E. Grove, A. P. McMahon, A local Wnt-3a signal is required for development of the mammalian hippocampus. *Development* **127**, 457–467 (2000).
61. H. Li *et al*., Itch promotes the neddylation of JunB and regulates JunB-dependent transcription. *Cell. Signal.* **28**, 1186–1195 (2016).
62. K. Mizutani, K. Yoon, L. Dang, A. Tokunaga, N. Gaiano, Differential Notch signalling distinguishes neural stem cells from intermediate progenitors. *Nature* **449**, 351–355 (2007).
63. C. Hanashima, S. C. Li, L. Shen, E. Lai, G. Fishell, Foxg1 suppresses early cortical cell fate. *Science* **303**, 56–59 (2004).